Desalination and Water Treatment
www.deswater.com

doi: 10.5004/dwt.2018.21805

102 (2018) 124–133
January

The fabrication of pentaerythritol pillared graphene oxide composite and its adsorption performance towards metal ions from aqueous solutions

Bao-Yu Yue, Lin-Yan Yu, Fei-Peng Jiao, Xin-Yu Jiang, Jin-Gang Yu*

College of Chemistry and Chemical Engineering, Hunan Provincial Key Laboratory of Efficient and Clean Utilization of Manganese Resources, Central South University, Changsha 410083, Hunan, China, Tel. +86 731 88879616; emails: yujg@csu.edu.cn (J.G. Yu), 775498809@qq.com (B.Y. Yue), 794643189@qq.com (L.Y. Yu), jiaofp@163.com (F.P. Jiao), jiangxinyu@csu.edu.cn (X.Y. Jiang)

Received 28 July 2017; Accepted 12 December 2017

ABSTRACT

Pentaerythritol-modified graphene oxide (GO-PER) composite was prepared by an esterification reaction. The chemical composition and morphology of the GO-PER composite were characterized by Fourier transform infrared (FT-IR) spectroscopy, thermogravimetric analysis, scanning electron microscopy, Brunauer–Emmett–Teller method, X-ray photoelectron spectroscopy (XPS) and Raman spectroscopy. The GO-PER composite was used as an efficient adsorbent for the removal of Pb(II) from aqueous solutions. Batch experiments were conducted to assess the effect of pH, temperature and contact time on the adsorption of Pb(II) onto the GO-PER composite. The adsorption kinetics, isotherms, and thermodynamics of Pb(II) onto the GO-PER composite were discussed in detail. The experimental data were fitted well by the pseudo-second-order kinetics model and Langmuir isotherm model, and the maximum adsorption capacity of GO-PER for Pb(II) was 126.9 mg g^{-1}. Values of various adsorption thermodynamic parameters, such as Gibbs free energy (ΔG^{θ}), entropy (ΔS^{θ}) and enthalpy (ΔH^{θ}), for adsorption of Pb(II) on GO-PER were calculated. Chemisorption was confirmed by FT-IR spectrum and XPS of GO-PER with adsorbed Pb(II). Thermodynamical study indicated that the adsorption of Pb(II) onto GO-PER was a spontaneous, endothermal, physical and monolayer process. The maximum adsorption capacities of GO-PER for trivalent lanthanum [La(III)], trivalent yttrium [Y(III)], trivalent erbium [Er(III)] and trivalent neodymium [Nd(III)] were 36.5, 32.375, 33.75 and 49.875 mg g^{-1}, respectively.

Keywords: Graphene oxide; Pentaerythritol; Composite; Adsorption; Metal ion

1. Introduction

Nowadays, the industrial wastewater discharged from many factories (such as chemical smelting industry, battery industry and mining industry) contain various toxic metal ions mainly as lead (Pb), copper (Cu), cadmium (Cd), chromium (Cr), zinc (Zn), rare earth elements and so on [1–4]. The metal ions can be accumulated in living organisms. If metal ions are ingested beyond the permitted concentration, they can cause serious health disorders [5]. Up to now, metal ion pollution is one of the most important factors that affect the environment. Therefore, it has received extensive attention throughout the world [6–9]. It is imperative to rigorously remove toxic metal contaminants prior to direct discharge into public sewers. Most importantly, the removal of these pollutants can not only protect the natural environment but also prevent effectively their accumulation in soils and aquatic environment and prevent their subsequent transfer through the food chain.

The current methods that have been used to treat metal-polluted water or wastewater streams include

* Corresponding author.

precipitation [10], membrane filtration [11], ion exchange [12] and adsorption [13]. The adsorption processes have been widely used for the removal of toxic metal ions from wastewater due to their effectiveness and cost-effectiveness [14–20]. Up to now, various adsorbents such as activated carbon, zeolite molecular sieve, resin and other inorganic materials have been developed [21,22]. However, the poor adsorbability and the relative low adsorption capacities of the materials motivate people to develop novel adsorbents which possess better properties such as more eco-friendly, lower cost and more efficient [23–25].

Because of their strong reactivity, large specific surface area and metal-chelating property, carbon nanomaterials have played important roles in wastewater treatment. Among the developed carbon nanomaterials, graphene has shown high adsorption capacities for metal ions. Several difficulties such as poor water dispersibility and agglomeration hinder the widespread application of graphene. Graphene oxide (GO) has a better prospect of application due plenty of hydrophilic functional groups such as hydroxyl, carbonyl, carboxyl and epoxy group on its surface. Besides providing more sites which are available for high-affinity adsorption for the metal ion species, the oxygen-containing groups of GO allow a large pool of functional molecules to be connected to GO [26], and the number of metal ion binding sites would be greatly increased [27,28]. Due to its four identical hydroxyl (–OH) groups, it is feasible to fabricate novel composites by grafting pentaerythritol (PER) onto carbon nanomaterials [29]. Furthermore, it is also expected that PER-modified carbon nanomaterials could provide more coordination sites for binding metal ions and possess relatively higher capacity for the adsorption of metal ions.

The GO-based adsorbents have shown potential application prospects, and the fabrication of GO-PER composite and the application of it in metal ion removal were rarely studied. Therefore, we hope to develop a novel adsorbent by preparation of this novel composite and evaluating its adsorption performance. Herein, the PER-modified GO (GO-PER) composite was fabricated and characterized, and it was used as a novel adsorbent for removal of bivalent lead [Pb(II)], trivalent lanthanum [La(III)], trivalent yttrium [Y(III)], trivalent erbium [Er(III)] and trivalent neodymium [Nd(III)] from aqueous solutions. The adsorption dynamics, thermodynamics and isotherms of the GO-PER composite for Pb(II) were discussed, and the adsorption mechanism was also proposed.

2. Experiments

2.1. Materials and measurements

Flake graphite and PER were obtained from Tianjin Kermel Chemical Reagent Development Center (Tianjin, China). Dimethyl sulfoxide (DMSO) was purchased from Tianjin Hengxing Chemical Reagent Co., Ltd., China. Yttrium chloride (YCl_3), neodymium chloride ($NdCl_3$), lanthanum chloride ($LaCl_3$), erbium chloride ($ErCl_3$), 1-(3-dimethylaminopropyl)-3-ethylcarbodiimide HCl (EDC·HCl) and 4-dimethylaminopyridine (DMAP) were purchased from Sinopharm Chemical Reagent Co., Ltd., China. All reagents and chemicals used in the experiments were of analytical grade and used without further purification.

2.2. Preparation of GO

The preparation of GO nanosheets was carried out by using natural flake graphite as a base material via an improved Hummers' method. First, a mixture of H_2SO_4 (98%; 36 mL) and H_3PO_4 (9 mL) was dropwise added into a mixture of flake graphite (300 mg) and $KMnO_4$ (1.5 g). The reaction mixture was vigorously stirred and maintained in an ice-water bath for another 10 min. The reaction flask was then transferred into an oil bath and stirred for 12 h at 50°C. Afterwards, the reaction mixture was naturally cooled down to room temperature. And 150 mL of deionized water and 3 mL of hydrogen peroxide (H_2O_2; 30%) were added to the flask to form a bright yellow mixture, which was subsequently stirred for another 30 min. The final product was obtained by repeatedly centrifuging and washing the suspension with 1 M hydrochloric acid and deionized water to remove the residual acid and other ions, and a freeze-drying procedure.

2.3. Preparation of GO-PER

The GO-PER nanocomposite was prepared as follows: first, a well-dispersed suspension was obtained by ultrasonic treatment of 300 mg of GO, 100 mg of DMAP and 500 mg of EDC·HCl in 50 mL of anhydrous DMSO for 10 min. Then 2 g of PER was added into the reaction mixture, and the reaction flask was placed into an oil bath and stirred for 30 h at 60°C. The GO-PER nanocomposite could be obtained by repeated filtration and washing with deionized water and ethanol, and finally a freeze-drying procedure.

2.4. Characterization

The chemical composition of GO-PER was confirmed by Fourier transform infrared (FT-IR) spectroscopy. FT-IR spectra for GO-PER were recorded in the range of 400–4,000 cm^{-1} with a resolution of 8 cm^{-1} on a Nicolet-Avatar 360 FT-IR spectrometer (Nicolet Corporation, USA); Raman spectra analysis was carried out using a micro-Raman spectrometer (Renishawplc (Gloucestershire, UK) Ramascope-2000) which operated at 514.5 nm. Thermogravimetric analysis (TGA) was carried out on a TA Instruments DSC 2910 which was controlled by a TA Instruments 2100 system in the temperature range of 25°C–800°C with a heating rate of 10°C min^{-1} in argon (Ar) atmosphere. Field emission scanning electron microscopy images of GO and GO-PER samples were obtained using a MIRA3 TESCAN electron microscope (MIRA3 TESCAN, UK) operating at 15 kV. The Brunauer–Emmett–Teller (BET) surface area of GO-PER was analyzed by a surface area detecting instrument (Kubo X1000) analyzer. X-ray photoelectron spectroscopy (XPS) analysis was performed on a Thermo Fisher Scientific K-Alpha XPS spectrometer (Thermo Fisher Scientific Inc., USA) in the spectral range of 0–1,350 eV with an Ar^+ beam sputtering. The BET surface area of GO-PER before and after adsorption of Pb(II) was analyzed by a surface area detecting instrument (Kubo X1000) analyzer.

2.5. Batch adsorption experiments

Batch adsorption experiments were carried out by agitating 4.0 mg of adsorbent with 50.00 mL of Pb(II) solutions

with different initial concentrations (10–100 mg L^{-1}). The remaining concentrations of Pb(II) after adsorption were determined by inductively coupled plasma atomic emission spectroscopy. The experimental conditions such as contact time, pH values, temperature and initial Pb(II) concentrations were investigated. The equilibrium adsorption capacity (q_e. mg g^{-1}) and percentage removal of Pb(II) (R, %) for all experiments were determined by the following equations, respectively:

$$q_e = \frac{(C_0 - C_t) \times V}{m} \quad (1)$$

$$R(\%) = \frac{(C_0 - C_t)}{C_0} \times 100 \quad (2)$$

where C_0 (mg L^{-1}) is the initial Pb(II) concentration; C_e (mg L^{-1}) is the equilibrium concentration of Pb(II); V (L) is the volume of Pb(II), while m (g) is the mass of GO-PER; R (%) is the percentage removal of Pb(II).

3. Results and discussion

3.1. Characterization

As shown in Fig. 1, the surface morphologies of as-prepared GO and GO-PER were observed by scanning electron microscopy (SEM). GO exhibits paper-thin, flexible and lightweight morphology features (Fig. 1(A)). After modified with the pentaerythritol, the GO-PER shows a multilayer stack structure of layers (Fig. 1(B)). Compared with the smooth surface of GO at high magnification (Fig. 1(C)), the GO-PER exhibits thin wrinkled sheets with rolled-up edges, indicating the successful surface grafting of PER (Fig. 1(D)). Due to the adsorption of Pb(II), the surface of GO-PER after adsorption is becoming roughened (Fig. 1(E)), which can restore to its original morphology (Fig. 1(F)) by soaking GO-PER with 0.05 M nitric acid, washing it repeatedly with deionized water and then freeze drying at –50°C.

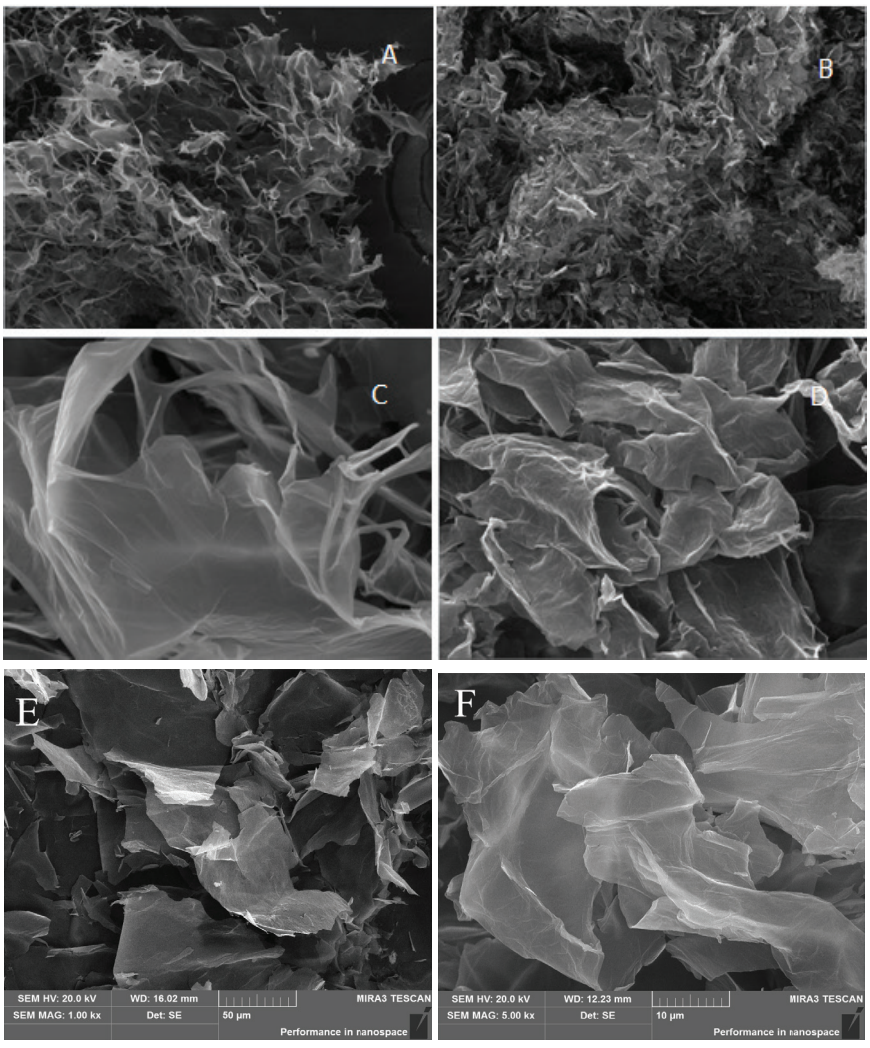

Fig. 1. SEM images of GO with scale bars are 100 nm for (A) and 10 nm for (C), respectively; and SEM images of GO-PER with scale bars are 100 nm for (B) and 10 nm for (D), respectively; (E) SEM image of GO-PER after adsorption of Pb(II); (F) SEM image of GO-PER after desorption.

In order to confirm the grafted PER components of GO-PER composite, FT-IR spectra were applied to identify the functional groups. As shown in Fig. 2(A), it can be observed that the peaks at 1,100 and 1,140 cm^{-1} which correspond to the C–O stretching vibration of carboxylic acids and epoxide, suggesting that GO possesses oxygen-containing groups such as carboxyl and epoxy [30–32]. If GO was functionalized with PER, these peaks disappeared due to the formation of ester groups and the epoxide ring-opening reaction (Fig. 2(B)). Furthermore, the emerging peak at 1,739 cm^{-1} could be ascribed to the C=O stretching vibration of the ester group. Meanwhile, the peak at 1,219 cm^{-1} could be attributed to the stretching vibration of C–O–C bond of the ester group. Therefore, PER was successfully grafted onto the surface of GO by the formation of ester bonds.

GO and GO-PER were also analyzed using Raman scattering spectroscopy. As shown in Fig. 3(A,a), the two characteristic peaks of GO, D band (1,359 cm^{-1}) and G band (1,584 cm^{-1}), are displayed in Raman spectra, which are corresponding to sp^3 carbon atoms of the defect structure and sp^2 hybridized carbon atoms of the aromatic rings, respectively. Compared with GO, the intensity ratio of D band and G band (I_D/I_G) of GO-PER increased, indicating many defects were created during the grafting procedure (Fig. 3(A,b)) [33].

The GO-PER was pyrolyzed from room temperature to 800°C in an argon (Ar) atmosphere. Fig. 3(B) shows the TGA curve of GO-PER, which indicates a four-stage weight loss in the temperature range 25°C–150°C, 150°C–200°C, 180°C–200°C, 200°C–350°C and 350°C–800°C. The overall percentage weight loss was around 65%. Nearly a 9.3% weight loss has occurred at 100°C which is corresponding to de-intercalation of water from the gallery space of the GO-PER composite. The 21.7% weight loss near 200°C for the GO-PER composite is presumably due to the pyrolysis of the grafted PER. After 200°C, the 20.7% weight loss has occurred for GO-PER composite due to decomposition of the oxygen-containing groups of the GO such as hydroxyl (–OH), carboxyl (–COOH), epoxy (–C–O–C–) and carbonyl (–C=O) groups [34,35]. Finally, a slow weight loss (8.3%) at the high temperature (>350°C) can be observed, which can be assigned to the pyrolysis of GO. All the observations have revealed that the GO-PER composite still possessed relatively high thermal stability.

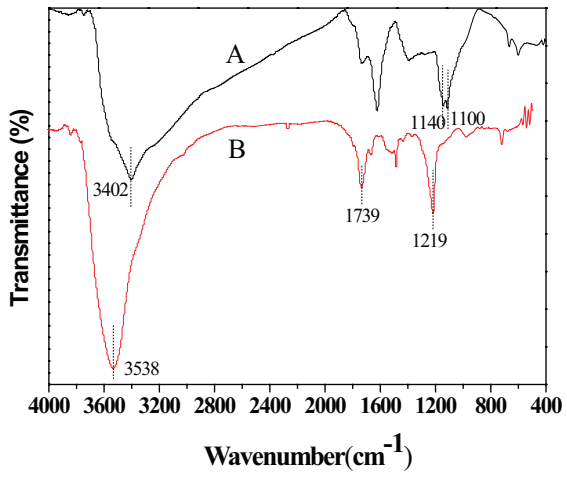

Fig. 2. FT-IR spectra of the samples: (A) GO; (B) GO-PER.

The BET surface area of GO-PER before and after adsorption were determined by applying the theory of nitrogen (N_2) adsorption isotherms measured at 77 K (Fig. 4). Typical

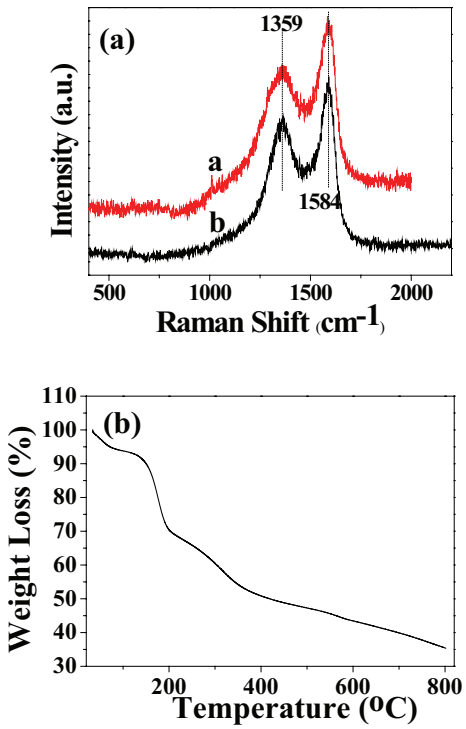

Fig. 3. (a) Raman spectra of the samples: (a) GO, (b) GO-PER; (b) TGA curve of GO-PER.

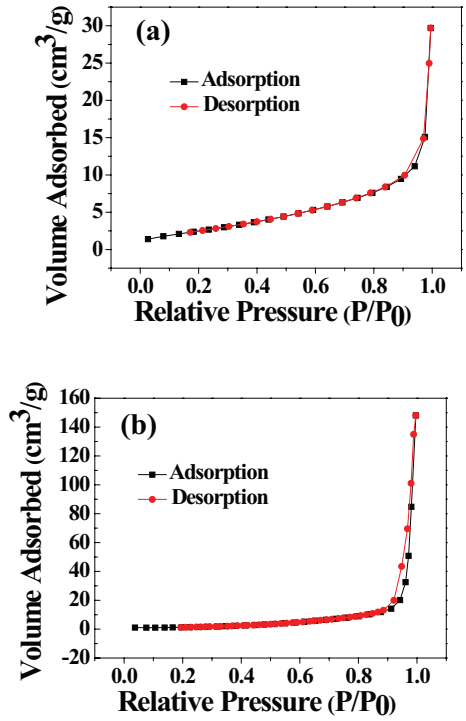

Fig. 4. N_2 adsorption/desorption isotherms of GO-PER; (a) before adsorption; (b) after adsorption.

experimental adsorption isotherms of type III have been obtained for the two GO-PER samples. The specific surface area of GO-PER before adsorption was 10.1 $m^2 g^{-1}$, which decreased to 4.4 $m^2 g^{-1}$ after adsorption of Pb(II). The interaction of Pb(II) with GO-PER would increase its unit weight per unit volume. As a result, the specific surface area of GO-PER decreased after adsorption of Pb(II).

3.2. Pb(II) adsorption on GO-PER: effects of contact time, pH and initial concentration

The influence of contact time on the removal of Pb(II) by GO-PER was investigated. As shown in Fig. 5(A), the adsorption capacity of Pb(II) on GO-PER increased rapidly during the first 20 min. And the adsorption capacity kept almost unchanged for approximately 40 min, indicating the adsorption equilibrium was reached.

Because of the solubility product constant of $Pb(OH)_2$ (K_{sp} = 1.2 × 10^{-15}), Pb(II) would precipitate at pH ≥ 8.4. To investigate the effects of pH on Pb(II) adsorption by GO-PER, the initial solution pH values were set in the range of 1.0 to 7.0. Fig. 5(B) shows the effects of pH on the adsorption of Pb(II) by GO-PER. Obviously, the adsorption capacities of GO-PER towards Pb(II) increased with an increase of pH value. The competitive adsorption between Pb(II) and hydrogen ion (H^+) in the solutions decreased with an increase of the solution pH, thus the adsorption capacity of GO-PER for Pb(II) increased.

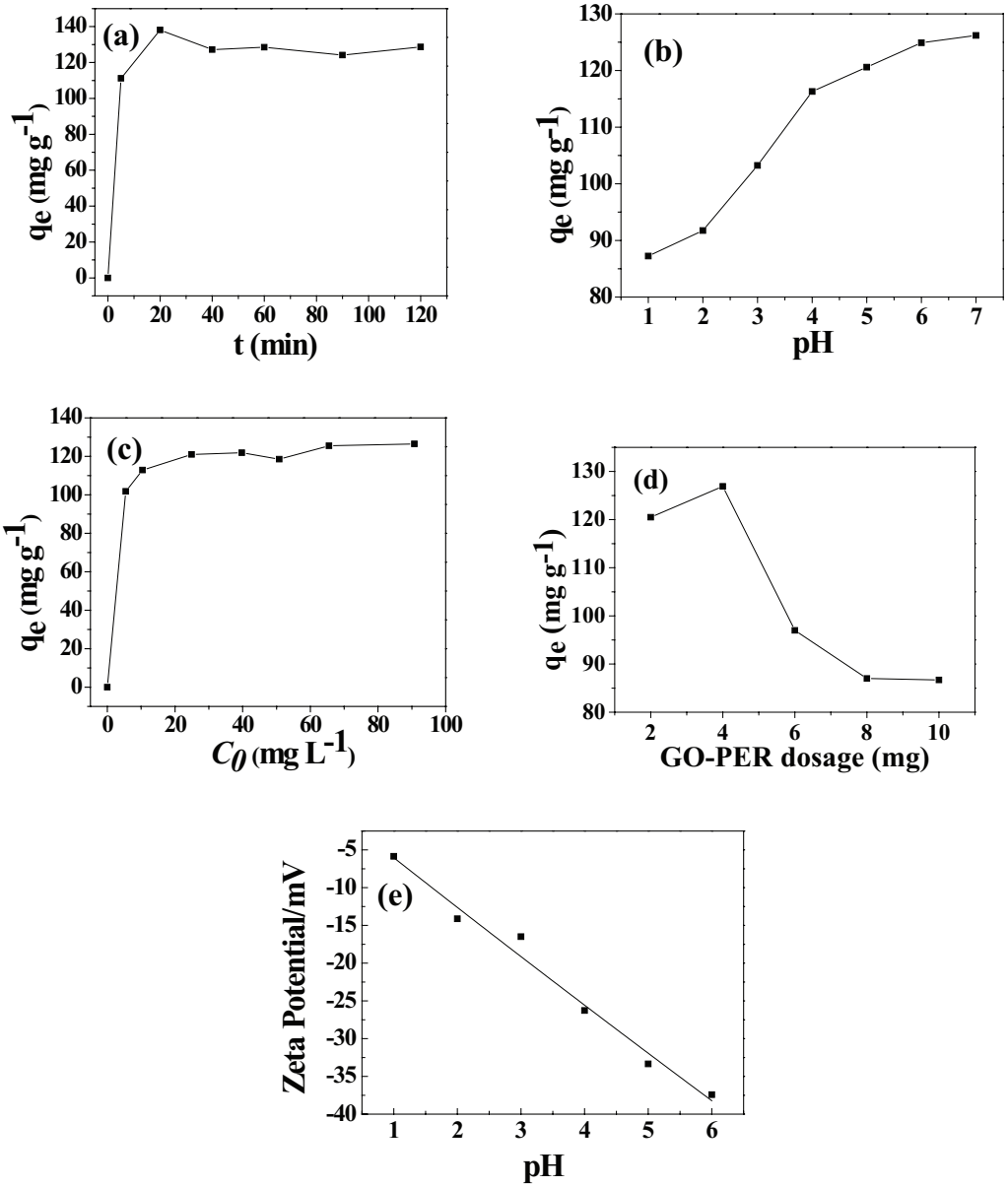

Fig. 5. Effects of contact time (A), pH (B) and initial Pb(II) concentrations (C) on the adsorption of Pb(II) onto GO-PER at 298.15 K (C_0 = 50.00 mg L^{-1}; GO-PER dosage = 80 mg L^{-1}); (D) Effects of GO-PER dosage on the adsorption of Pb(II) onto GO-PER at 298.15 K (C_0 = 50.00 mg L^{-1}); (E) Zeta potential of GO-PER at various pH values.

In addition, the oxygen-containing groups on the surface of GO-PER can form metal–ligands with Pb(II) due to the chelate efforts and Lewis acid-base interactions. The following adsorption experiments were conducted in the solutions of pH 7.0.

The concentration of metal ion present in water is an important factor affecting the removal efficiency of GO-PER. Therefore, effects of seven gradient initial Pb(II) concentrations (10–100 mg L^{-1}) on the removal efficiency were investigated. As shown in Fig. 5(C), q_e value increases as initial concentration increases and finally tended to be stable. The maximum q_e achieves a relative stable value of 126.9 mg g^{-1} at an initial Pb(II) concentration of higher than 30 mg g^{-1}.

50.00 mL of the Pb(II) solution was mixed with different dosage of adsorbent (2, 4, 6, 8 and 10 mg) and oscillated at 298.15 K for 60 min. As shown in Fig. 5(D), the GO-PER composite showed maximum adsorption capacity of 126.9 mg g^{-1} for the addition of 4.0 mg of adsorbent. It can be observed that the q_e increases and reached the maximum and finally decreases. The enhancement of the adsorption capacity maybe due to the increase in the available active sites for the Pb(II) adsorption. The q_e decreases with further increasing the dosage, which might be due to the fact that the transportation of Pb(II) ions to the active adsorption sites will be limited [19,25].

Zeta potentials have been widely used to characterize the particle surface charges. To understand the interaction between GO-PER and Pb(II), the zero point of charge (pHzpc) of GO-PER was determined by measuring its zeta potential in aqueous solution as a function of pH. As shown in Fig. 5(E), the zeta potentials of GO-PER are negative and the pHzpc is at pH < 0, and the amount of negative charges increases with increasing pH, indicating that the surface charge of GO-PER is negative over a wide pH range, which may be beneficial for cationic sorption. And electrostatic interaction can thus be the primary driving force for the adsorption of metal ions by the adsorbent.

3.3. Adsorption kinetics

To determine the rate of the adsorption process, two kinetic reaction models including pseudo-first-order model and pseudo-second-order model were used to investigate the experimental data (Fig. 6).

The pseudo-first-order model is shown as follows:

$$\ln\left(q_e - q_t\right) = \ln q_t - k_1 t \tag{3}$$

where q_e (mg g^{-1}) is the equilibrium absorption capacity of Pb(II) and q_t (mg g^{-1}) is the amount of Pb(II) adsorbed on the adsorbent at time t (min); and k_1 (min^{-1}) is the pseudo-first-order rate constant.

The pseudo-second-order model can be expressed as follows:

$$\frac{t}{q_t} = \frac{1}{k_2 q_e^{\,2}} + \frac{1}{q_e} t \tag{4}$$

where k_2 (g mg^{-1} min^{-1}) is the pseudo-second-order rate constant.

As listed in Table 1, the fitting parameters indicated that the sorption process fitted well to the pseudo-second-order model with maximum monolayer adsorption capacity of 127.1 mg g^{-1}, which is closer to the experimental q_e value than that obtained from pseudo-first-order model.

3.4. Adsorption isotherms

To describe the relationship between the amounts of adsorbate adsorbed on the adsorbents and the concentrations of dissolved adsorbates in the solution at equilibrium, several adsorption isothermal equations have been published in the literature and widely used to describe the adsorption

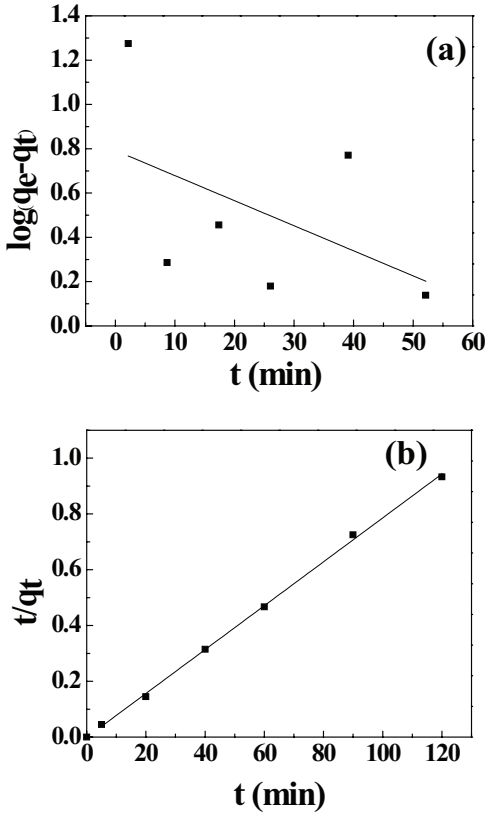

Fig. 6. Adsorption kinetics of Pb(II) onto GO-PER (C_0 = 50.00 mg L^{-1}; GO-PER dosage = 80 mg L^{-1}): (a) pseudo-first-order model; (b) pseudo-second-order model.

Table 1
Kinetic parameters of Pb(II) adsorption onto GO-PER (C_0 = 50.00 mg L^{-1}; GO-PER dosage = 80 mg L^{-1})

Pseudo-first-order model		Pseudo-second-order model			
k_1 (h^{-1})	R^2	k_2 (mg g^{-1} $h^{0.5}$)	R^2	$q_{e,exp}$ (mg g^{-1})	$q_{e,cal}$ (mg g^{-1})
0.01132	0.4856	0.05735	0.9986	124.1	127.1

experimental data [36,37]. Two most frequently used models, Langmuir model and Freundlich model, were applied to study the adsorption experimental data. As shown in Fig. 7 and Table 2, the adsorption of Pb(II) onto GO-PER is well fitted by the Langmuir isotherm model with maximum monolayer adsorption capacity of 126.9 mg g^{-1}. The results are in accordance with the previously reported results obtained from other functionalized GO composites [38–40]. Additionally, GO-PER possessed higher maximum adsorption capacity for Pb(II) than most of the previously reported graphene-based adsorbents. And it also showed higher adsorption capacities of 36.5, 32.375, 33.75 and 49.875 mg g^{-1} for La(III), Y(III), Er(III) and Nd(III), respectively, illustrating its potential applications in removal of metal ions from aqueous solutions (Table 3).

3.5. Adsorption thermodynamics

To investigate the degree of the spontaneity of the adsorption process, the thermodynamic parameters including Gibbs free energy change (ΔG^{θ}), Enthalpy change (ΔH^{θ}) and entropy change (ΔS^{θ}) were calculated by the following equations [46].

$$K_c = \frac{C_a}{C_b} \tag{5}$$

$$\Delta G^{\theta} = -RT \ln K_c \tag{6}$$

$$\ln K_c = \frac{\Delta S^{\theta}}{R} - \frac{\Delta H^{\theta}}{RT} \tag{7}$$

where K_c is the distribution coefficient for the adsorption; R (8.314 J mol^{-1} K^{-1}) is the universal gas constant; T is the absolute temperature; C_a (mg L^{-1}) is the concentration of solute adsorbed on the adsorbent at equilibrium, and C_b (mg L^{-1}) is the equilibrium adsorbate concentration in the aqueous phase.

As listed in Table 4, it can be seen that the adsorption capacity increased with an increase of the solution temperature. And the negative ΔG^{θ} values indicate that the adsorption process is spontaneous. The positive ΔH^{θ} value

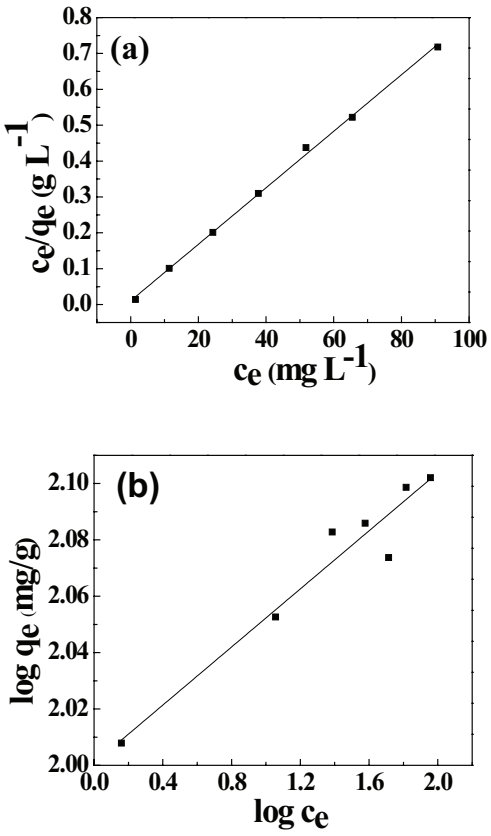

Fig. 7. Adsorption isotherms of Pb(II) onto GO-PER: (a) Langmuir isotherm model; (b) Freundlich isotherm model.

Table 2
Isotherm parameters for Pb(II) adsorption on GO-PER

Model	Parameters	Parameter values
Langmuir	q_m (mg g^{-1})	126.9
	k_L (L mg^{-1})	0.7462
	R^2	0.9984
Freundlich	$1/n$	0.05154
	k_F ([(mg g^{-1})(mg L^{-1})$^{-1}$ n^{-1}])	100.2
	R^2	0.9268

Table 3
The adsorption capacities of previously reported adsorbents for metal ions

Adsorbent	Metal ions	q_m (mg g^{-1})	Reference
3D Mg–Al layered double hydroxide/ partially reduced GO	Pb(II)	116.2	[41]
Multi-layered oxidized graphene	Pb(II)	103	[42]
Paste of few-layered oxidized graphene	Pb(II)	38	[42]
L-glutamic acid modified GO	Pb(II)	513.4	[43]
Dibromocarbene modified graphene	Pb(II)	49.46	[44]
Diiodocarbene modified graphene	Pb(II)	49.36	[45]
GO-PER	Pb(II), La(III), Y(III), Er(III) and Nd(III)	126.9, 36.5, 32.375, 33.75 and 49.875, respectively	This work

Table 4
Thermodynamic parameters for the adsorption of Pb(II) on GO-PER

Parameters	T (K)	$\frac{\Delta G^{\theta}}{RT}$ (kJ mol^{-1})	ΔH^{θ} (kJ mol^{-1})	ΔS^{θ} (J mol^{-1} K^{-1})
GO-PER	298	–20.03		
	308	–20.80	2.302	77.54
	318	–21.58		

describes an endothermic adsorption process. The positive ΔS^{θ} value shows that the adsorption is an entropy increasing process. Therefore, the adsorption of Pb(II) onto GO-PER is a spontaneous, endothermic and entropy increasing process.

3.6. Regeneration of adsorbent

For regenerating GO-PER, 0.05 M nitric acid was used to treat the adsorbent after adsorption. The same adsorption procedures as described above were performed for the recycled adsorbent. And five cycles of regeneration were conducted under the same experimental conditions. It was revealed that GO-PER could be successfully recycled for five times with less than 15% total loss in adsorption capacity. The grafting of PER contributed a lot to the regeneration and assisted the regenerated adsorbent to be more effective.

3.7. Adsorption mechanism

The adsorption process might be primarily driven by electrostatic forces due to the surface charge of GO-PER is negative over a wide pH range. Then it can be seen from the structures of GO that it possesses abundant oxygen-containing groups including hydroxyl (–OH), carbonyl (–COOH) and epoxy (–C–O–C–) on the surface. These functional groups can react with metal ions to form coordination bonds due to their lone-pair electrons. The covalent grafting of PER can introduce a mass of –OH groups onto GO, increasing the possible coordination interactions between metal ions and GO-PER. The absorption peak of C=O of GO-PER shifts from 1,739 cm^{-1} (Fig. 3(B)) towards lower wavenumbers at 1,715.88 cm^{-1} after adsorption of Pb(II) (Fig. 8(A)), we can get a conclusion that there were coordination interactions between GO-PER and Pb(II). The interactions between GO-PER and Pb(II) were further confirmed by XPS (Fig. 8(B)). The XPS spectrum of GO-PER before adsorption shows four peaks at 282.0, 284.5, 285.2 and 287.6 eV which can be assigned to C=C, C–C, C–O and C=O bonds, respectively. These functional groups are associated with the graphitic carbon and the carboxylic and/or ester groups of GO-PER. The C1s spectrum of GO-PER after adsorption also reveals four peaks at 283.9 eV (C=C), 285.2 eV (C–C), 286.8 eV (C–O) and 289.0 eV (C=O), respectively. The doublets characteristic peaks observed at 138.18 (assigned to Pb $4f_{7/2}$) and at 143.14 eV (assigned to Pb $4f_{5/2}$) agree with the reported values for PbO, indicating a fixation of Pb(II) onto GO-PER after loading with Pb(II) solution [47].

In addition, the tetrahedron structure of PER may enlarge the distance between GO sheets, which can increase the specific surface area of GO-based composites and be beneficial to improve their adsorption capacities. Furthermore,

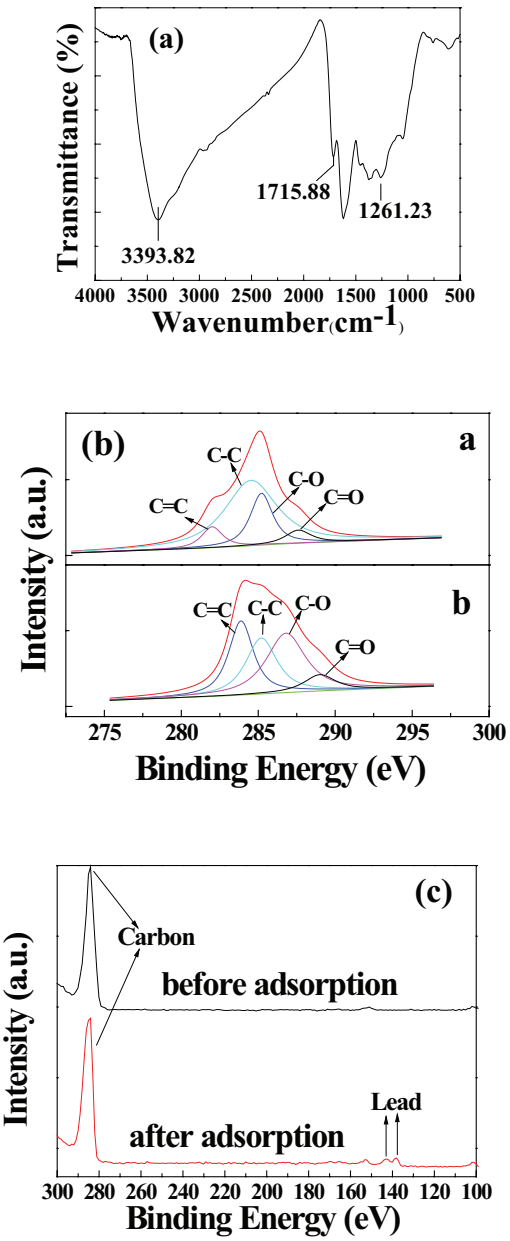

Fig. 8. (a) FT-IR spectra of GO-PER after adsorption of Pb(II); (b) C1s XPS of GO-PER before (a) and after (b) adsorption of Pb(II); (c) Pb 4f XPS of GO-PER before (a) and after (a) adsorption of Pb(II).

the delocalized π-electrons in six-membered aromatic and quasi-aromatic rings of GO-PER can form Lewis acid-base pairs with metal ions. All of the above-mentioned interactions contribute to the adsorption capacity of GO-PER for metal ions (Fig. 9).

4. Conclusions

The preparation and purification of GO-PER was carried out, which was used as an efficient adsorbent for the removal of Pb(II), La(III), Y(III), Er(III) and Nd(III) from aqueous solutions. The GO-PER was characterized by FT-IR

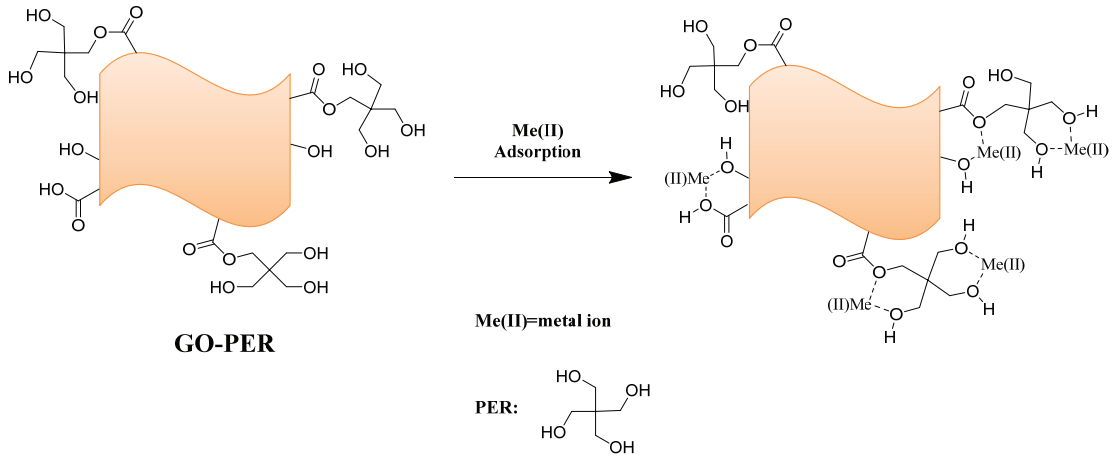

Fig. 9. Proposed mechanism for the adsorption of metal ions onto GO-PER.

spectroscopy, Raman spectroscopy, SEM, XPS and TGA. The adsorption kinetics and isomers are well fitted by the pseudo-second-order model and Langmuir isotherm model, respectively. The obtained thermodynamic parameters indicated that the adsorption of Pb(II) onto GO-PER was a spontaneous, endothermic and entropy increasing process. We also proposed the possible adsorption mechanisms, and the coordination interactions and Lewis acid-base pairs between metal ions and GO-PER may contribute a lot to the highly efficient adsorption.

Acknowledgements

The financial supports from the National Natural Science Foundation of China (Nos. 51674292, 21471163 and 21571191), the Provincial Natural Science Foundation of Hunan (No. 2016JJ1023), the Project of Innovation-driven Plan in Central South University (No. 2016CX007), the Hunan Provincial Science and Technology Plan Project, China (No. 2016TP1007), and the Fundamental Research Funds for the Central Universities of Central South University (No. 2016zzts235) are greatly appreciated.

References

[1] L.A. Chai, X.B. Min, N. Tang, Y.Y. Wang, Mechanism and kinetics of Zn(II) removal from wastewater by immobilised beads of SRB sludge, Int. J. Environ. Pollut., 37 (2009) 20–33.
[2] L.Y. Chai, Y.N. Chen, Z.H. Yang, Kinetics and thermodynamics of arsenate and arsenite biosorption by pretreated spent grains, Water Environ. Res., 81 (2009) 843–848.
[3] J. Yang, L.Y. Chai, Y.Y. Wang, X.W. He, Transportation and distribution of chromium in the anaerobic sludge treating the chromium-containing wastewater, Int. J. Environ. Pollut., 38 (2009) 256–266.
[4] L.Y. Chai, Q.W. Wang, Q.Z. Li, Z.H. Yang, Y.Y. Wang, Enhanced removal of Hg(II) from acidic aqueous solution using thiol-functionalized biomass, Water Sci. Technol., 62 (2010) 2157–2166.
[5] G. Chen, K.J. Shah, L. Shi, P.-C. Chiang, Removal of Cd(II) and Pb(II) ions from aqueous solutions by synthetic mineral adsorbent: performance and mechanisms, Appl. Surf. Sci., 409 (2017) 296–305.
[6] A. Garcia-Sanchez, A. Alastuey, X. Querol, Heavy metal adsorption by different minerals: application to the remediation of polluted soils, Sci. Total. Environ., 242 (1999) 179–188.
[7] Q.Z. Li, L.Y. Chai, Z.H. Yang, Q.W. Wang, Y.Y. Wang, A comparative study of Ag(I) adsorption on raw and modified spent grain: kinetic and thermodynamic aspects, Water Environ. Res., 82 (2010) 2290–2296.
[8] Y.Y. Wang, B. Peng, Z.H. Yang, C.J. Tang, Y.H. Chen, Q. Liao, Y.P. Liao, Treatment of Cr(VI) contaminated water with *Pannonibacter phragmitetus* BB, Environ. Earth Sci., 71 (2014) 4333–4339.
[9] T. Wang, L.Y. Zhang, C.F. Li, W.C. Yang, T.T. Song, C.J. Tang, Y. Meng, S. Dai, H.Y. Wang, L.Y. Chai, J. Luo, Synthesis of core-shell magnetic Fe_3O_4@poly(m-phenylenediamine) particles for chromium reduction and adsorption, Environ. Sci. Technol., 49 (2015) 5654–5662.
[10] H. Sis, T. Uysal, Removal of heavy metal ions from aqueous medium using Kuluncak (Malatya) vermiculites and effect of precipitation on removal, Appl. Clay Sci., 95 (2014) 1–8.
[11] M. Mhamdi, E. Elaloui, M. Trabelsi-Ayadi, Adsorption of zinc by a Tunisian Smectite through a filtration membrane, Ind. Crop. Prod., 47 (2013) 204–211.
[12] M.D. Victor-Ortega, J.M. Ochando-Pulido, G. Hodaifa, A. Martinez-Ferez, Ion exchange as an efficient pretreatment system for reduction of membrane fouling in the purification of model OMW, Desalination, 343 (2014) 198–207.
[13] J. Teng, X. Zeng, X. Xu, J.G. Yu, Assembly of a novel porous 3D graphene oxide-Starch architecture by a facile hydrothermal method and its adsorption properties toward metal ions. Mater. Lett., 214 (2018) 31–33.
[14] A. Demirbas, Heavy metal adsorption onto agro-based waste materials: a review, J. Hazard. Mater., 157 (2008) 220–229.
[15] M. Naushad, T. Ahamad, B.M. Al-Maswari, A. Abdullah Alqadami, S.M. Alshehri, Nickel ferrite bearing nitrogen-doped mesoporous carbon as efficient adsorbent for the removal of highly toxic metal ion from aqueous medium, Chem. Eng. J., 330 (2017) 1351–1360.
[16] G. Sharma, M. Naushad, A.H. Al-Muhtaseb, A. Kumar, M.R. Khan, S. Kalia, Shweta, M. Bala, A. Sharma, Fabrication and characterization of chitosan-crosslinked-poly(alginic acid) nanohydrogel for adsorptive removal of Cr(VI) metal ion from aqueous medium, Int. J. Biol. Macromol., 95 (2017) 484–493.
[17] M. Naushad, T. Ahamad, G. Sharma, A.H. Al-Muhtaseb, A.B. Albadarin, M.M. Alam, Z.A. Alothman, S.M. Alshehri, A.A. Ghfar, Synthesis and characterization of a new starch/SnO_2 nanocomposite for efficient adsorption of toxic Hg^{2+} metal ion, Chem. Eng. J., 300 (2016) 306–316.
[18] A.A. Alqadami, M. Naushad, M.A. Abdalla, T. Ahamad, Z.A. Alothman, S.M. Alshehri, Synthesis and characterization of Fe_3O_4@TSC nanocomposite: highly efficient removal of toxic metal ions from aqueous medium, RSC Adv., 6 (2016) 22679–22689.
[19] M. Naushad, Z.A. Alothman, M.R. Awual, M.M. Alam, G.E. Eldesoky, Adsorption kinetics, isotherms, and thermodynamic

studies for the adsorption of Pb^{2+} and Hg^{2+} metal ions from aqueous medium using Ti(IV) iodovanadate cation exchanger, Ionics, 21 (2015) 2237–2245.
[20] C.F. Carolin, P.S. Kumar, A. Saravanan, G.J. Joshiba, M. Naushad, Efficient techniques for the removal of toxic heavy metals from aquatic environment: a review, J. Environ. Chem. Eng., 5 (2017) 2782–2799.
[21] A. Mittal, M. Naushad, G. Sharma, Z.A. Alothman, S.M. Wabaidur, M. Alam, Fabrication of MWCNTs/ThO_2 nanocomposite and its adsorption behavior for the removal of Pb(II) metal from aqueous medium, Desal. Wat. Treat., 57 (2016) 21863–21869.
[22] R. Bushra, M. Naushad, G. Sharma, A. Azam, Z.A. Alothman, Synthesis of polyaniline based composite material and its analytical applications for the removal of highly toxic Hg^{2+} metal ion: antibacterial activity against *E. coli*, Korean J. Chem. Eng., 34 (2017) 1970–1979.
[23] A. Gladysz-Plaska, E. Skwarek, T.M. Budnyak, D. Kolodynska, Metal ions removal using nano oxide pyrolox material, Nanoscale Res. Lett., 12 (2017) 95–95.
[24] M. Naushad, Z.A. Alothman, Inamuddin, H. Javadian, Removal of Pb(II) from aqueous solution using ethylene diamine tetra acetic acid-Zr(IV) iodate composite cation exchanger: kinetics, isotherms and thermodynamic studies, J. Ind. Eng. Chem., 25 (2015) 35–41.
[25] M. Naushad, Z.A. Alothman, Separation of toxic Pb^{2+} metal from aqueous solution using strongly acidic cation-exchange resin: analytical applications for the removal of metal ions from pharmaceutical formulation, Desal. Wat. Treat., 53 (2015) 2158–2166.
[26] J.G. Yu, B.Y. Yue, X.W. Wu, Q. Liu, X.Y. Jiang, M. Zhong, H.Y. Li, S.S. Li, X.Q. Chen, The covalently organic functionalization of graphene: methodologies and protocols, Curr. Org. Chem., 20 (2016) 1284–1298.
[27] B. Zawisza, A. Baranik, E. Malicka, E. Talik, R. Sitko, Preconcentration of Fe(III), Co(II), Ni(II), Cu(II), Zn(II) and Pb(II) with ethylenediamine-modified graphene oxide, Microchim. Acta, 183 (2016) 231–240.
[28] N. Chen, J. Teng, F. Jiao, X. Jiang, X. Hao, J. Yu, Preparation of triethanolamine functionalized carbon nanotube for aqueous removal of Pb(II), Desal. Wat. Treat., 71 (2017) 191–200
[29] J.Y. Yang, X.Y. Jiang, F.P. Jiao, J.G. Yu. The oxygen-rich pentaerythritol modified multi-walled carbon nanotube as an efficient adsorbent for aqueous removal of alizarin yellow R and alizarin red S. Appl. Surf. Sci., 436 (2018) 198–206.
[30] Y.Y. Zhu, H.J. Cui, S.P. Jia, J.F. Zheng, P.J. Yang, Z.J. Wang, Z.P. Zhu, 3D graphene frameworks with uniformly dispersed CuS as an efficient catalytic electrode for quantum dot-sensitized solar cells, Electrochim. Acta, 208 (2016) 288–295.
[31] J. Yu, J. Zou, L. Liu, X. Jiang, F. Jiao, X. Chen, Preparation of TiO_2 based photocatalysts and their photocatalytic degradation properties for methylene blue, rhodamine B and methyl orange, Desal. Wat. Treat., 81 (2017) 282–290.
[32] J.Y. Yang, X.Y. Jiang, F.P. Jiao, J.G. Yu, X.Q. Chen, Fabrication of diiodocarbene functionalized oxidized multi-walled carbon nanotube and its aqueous adsorption performance toward Pb(II), Environ. Earth Sci., 76 (2017) 677.
[33] Z.H. Wang, J.Y. Yang, X.W. Wu, X.Q. Chen, J.G. Yu, Y.P. Wu, Enhanced electrochemical performance of porous activated carbon by forming composite with graphene as high-performance supercapacitor electrode material, J. Nanopart. Res., 19 (2017) 77.
[34] Z.A. Wang, X.M. Zhang, X.W. Wu, J.G. Yu, X.Y. Jiang, Z.L. Wu, X. Hao, Soluble starch functionalized graphene oxide as an efficient adsorbent for aqueous removal of Cd(II): the adsorption thermodynamic, kinetics and isotherms, J. Sol-Gel Sci. Technol., 82 (2017) 440–449.
[35] T. Gao, J. Yu, Y. Zhou, X. Jiang, The synthesis of graphene oxide functionalized with dithiocarbamate group and its prominent performance on adsorption of lead ions, J. Taiwan Inst. Chem. Eng., 71 (2017) 426–432.
[36] C.H. Giles, D. Smith, A. Huitson, A general treatment and classification of the solute adsorption isotherm. I. Theoretical, J. Colloid Interface Sci., 47 (1974) 755–765.
[37] C.H. Giles, A.P. D'Silva, I.A. Easton, A general treatment and classification of the solute adsorption isotherm part. II. Experimental interpretation, J. Colloid Interface Sci., 47 (1974) 766–778.
[38] O. Karnitz, Jr., L.V. Alves Gurgel, J.C. Perin de Melo, V.R. Botaro, T.M. Sacramento Melo, R.P. de Freitas Gil, L.F. Gil, Adsorption of heavy metal ion from aqueous single metal solution by chemically modified sugarcane bagasse, Bioresour. Technol., 98 (2007) 1291–1297.
[39] M. Erdem, A. Ozverdi, Lead adsorption from aqueous solution onto siderite, Sep. Purif. Technol., 42 (2005) 259–264.
[40] M. Sekar, V. Sakthi, S. Rengaraj, Kinetics and equilibrium adsorption study of lead(II) onto activated carbon prepared from coconut shell, J. Colloid Interface Sci., 279 (2004) 307–313.
[41] G.B.B. Varadwaj, O.A. Oyetade, S. Rana, B.S. Martincigh, S.B. Jonnalagadda, V.O. Nyamori, Facile synthesis of three-dimensional Mg-Al layered double hydroxide/partially reduced graphene oxide nanocomposites for the effective removal of Pb^{2+} from aqueous solution, ACS Appl. Mater. Interface, 9 (2017) 17291–17306.
[42] A.E. Kucherova, I.V. Romantsova, A.E. Burakov, N.R. Memetov, M.N. Krasnyansky, Graphene-based nanocomposites for enhanced Pb^{2+} adsorption, Nano Hybrids Composites, 13 (2017) 323–329.
[43] H. Ge, W. Zou, Preparation and characterization of L-glutamic acid-functionalized graphene oxide for adsorption of Pb(II), J. Dispersion Sci. Technol., 38 (2017) 241–247.
[44] J. Teng, X. Zeng, B.Y. Yue, X.H. Zhao, Z.H. Wang, J.G. Yu, X.M. Xu, M. Zhong, X.W. Wu, W.X. Zhou, Z. Zhou, Dibromocarbene modified graphene: preparation, characterization and its application in removal of Pb(II) from aqueous solutions, Nanosci. Nanotechnol. Lett., 8 (2016) 226–231.
[45] H.Y. Li, B.Y. Yue, J.G. Yu, X.W. Wu, W.X. Zhou, N. Zhou, J. Teng, M. Zhong. Diiodocarbene modified graphene: Preparation, characterization and its application as a novel adsorbent for aqueous removal of Pb(II), Nanosci. Nanotechnol. Lett., 8 (2016) 387–392.
[46] X.H. Zhao, F.P. Jiao, J.G. Yu, Y. Xi, X.Y. Jiang, X.Q. Chen, Removal of Cu(II) from aqueous solutions by tartaric acid modified multi-walled carbon nanotubes, Colloid Surf., A, 476 (2015) 35–41.
[47] M.E. Counts, J.S.C. Jen, J.P. Wightman, Electron spectroscopy for chemical analysis study of lead adsorbed on montmorillonite, J. Phys. Chem., 77 (1973) 1924–1926.